Inorganic Chemistry

Article

pubs.acs.org/IC

Self-Assembly of Silver(I) and Gold(I) N-Heterocyclic Carbene Complexes in Solid State, Mesophase, and Solution

Tina H. T. Hsu,[†] Jaishri J. Naidu,[†] Bi-Jiuan Yang,[‡] Meng-Ying Jang,[†] and Ivan J. B. Lin*[,†]

[†]Department of Chemistry and Nanotechnology Research Center, National Dong Hwa University, Hualien, 974, Taiwan

[‡]Department of Chemistry, Fu-Jen Catholic University, Hsinchuang, Taipei, 242, Taiwan

Supporting Information

ABSTRACT: The assembly of silver(I) and gold(I) complexes of functionalized N-heterocyclic carbenes (NHCs) of the type $[M(C_n\text{amide-imy})_2][\text{anion}]$ were studied, in which $C_n$amide-imy stands for an NHC of imidazol-2-ylidene having one *N*-alkyl substituent (C_nH_{2n+1}) and one *N*-acetamido substituent, while the anions are Br^-, NO_3^-, BF_4^- or PF_6^-. A single crystal X-ray diffraction study reveals that self-assembly of $[Ag(C_{10}\text{amide-imy})_2][PF_6]$ through Coulombic, hydrogen bonding, and hydrophobic interactions gives a lamellar structure with tubular architecture around the metal ion head core. Self-assembly of these functionalized NHC complexes also leads to the formation of the first example of thermotropic liquid crystals of silver(I)−NHCs and gels of gold(I)−NHC. Results from an infrared spectroscopy study show that the degree of chain motion in the gel state is smaller than that in the mesophase, yet comparable to that in the solid state. In addition, the technique of nuclear magnetic resonance diffusion ordered spectroscopy was found for the first time to be a good tool to study the phase transition of gels. Xerogels of gold(I)−NHCs display fibers, oriental lantern-shaped bundles of belts and helical fibers when observed under scanning electron and transmission electron microscopes.

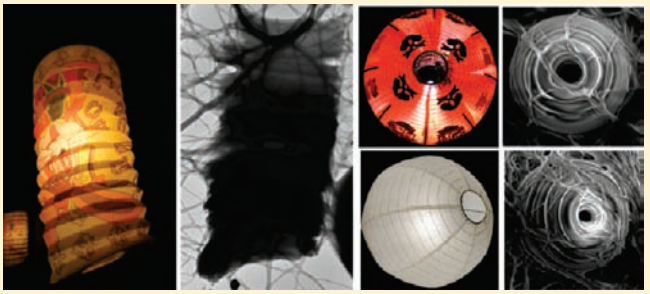

INTRODUCTION

Metal complexes of N-heterocyclic carbenes (NHCs) have been studied intensively in the last 20 years and have become a main stream in organometallic chemistry.[1] NHCs have been considered as superior alternatives to phosphines in many applications.[2−5] The primary characteristics of NHCs are their strong electron-donating ability, and their ability to form stable complexes with many metal ions.[6−10] Also, NHCs may be easily modified to tune their steric and electronic properties, a common strategy to improve catalyst activity and selectivity.[11,12] Other than their use as catalysts in chemical transformations, studies for other potential applications are limited.[13−15]

Molecules with suitable design may self-assemble through various intermolecular forces such as hydrogen bonding, dipole−dipole, $\pi-\pi$, and hydrophobic interactions to generate supramolecules in the solid state, and further to form liquid crystals (LCs) in mesophase, which represent a phase of matter that possesses liquid-like properties but with a certain degree of orientational order at the microscopic level. A typical example is 4-pentyl-4′-cyano-biphenyl (5CB), which has been used in LC displays.[16] Also as a class of LCs, ionic liquid crystals (ILCs) may exhibit many additional properties such as low vapor pressure and high ion conductivity other than orientational order.[17,18] Metal-containing liquid crystals (MLCs) with the presence of metal centers, can also confer still more properties on the LCs, such as electronic, magnetic, photonic, and even geometric.[19−32]

There have been a number of studies concerning the LCs based on imidazolium motifs,[33−41] however, reports of metal-NHC complexes derived from imidazolium ions are limited.[42,43] Although many silver(I)−NHCs with different ways of assembling were reported,[9] no liquid crystalline silver(I)-NHCs have been reported to date. In one case, a liquid crystalline material was obtained when a Ag(NHC)Cl complex was mixed at a 1:1 ratio with its corresponding imidazolium salt.[44]

"Gel" refers to the aggregation of highly anisotropic 3-D structures in solution, often through noncovalent interactions.[45,46] Steroid, amino acid or amide derivatives have been commonly employed to promote the formation of gels.[47−50] Various techniques such as nuclear magnetic resonance (NMR), powder X-ray diffraction (PXRD), scanning electron microscope (SEM), transmission electron microscopy (TEM), small-angle X-ray scattering (SAXS), and small-angle neutron scattering (SANS) have been employed to study the formation of gels.[51−53] Gels have been used to produce materials for optical,[54,55] electrical,[56] catalytic,[57] sensing,[58,59] chemical processing, foods, and drug delivery applications.[60−62] Recently, reviews on the incorporation of metal ions in gels appeared.[63,64]

Received: May 27, 2011
Published: December 2, 2011

 © 2011 American Chemical Society dx.doi.org/10.1021/ic2011343 | *Inorg. Chem.* 2012, 51, 98−108

Scheme 1. Synthesis of Silver(I)−NHC Complexes

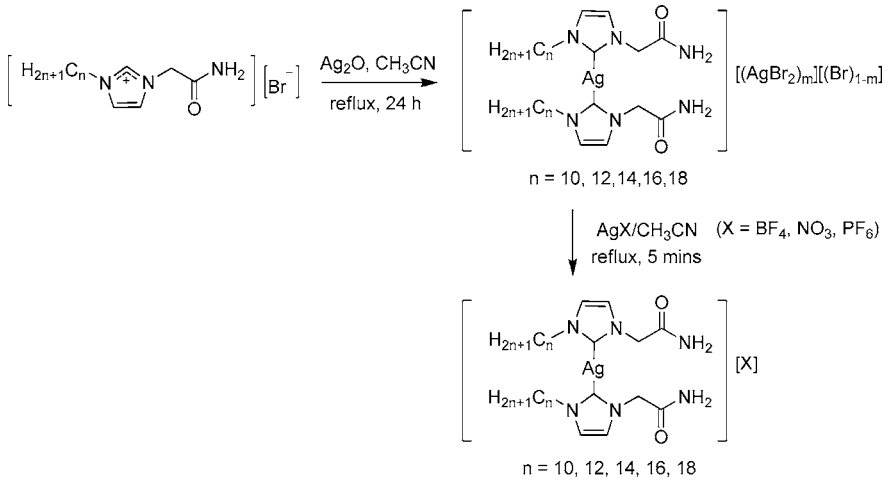

Scheme 2. Synthesis of Gold(I)−NHC Complexes

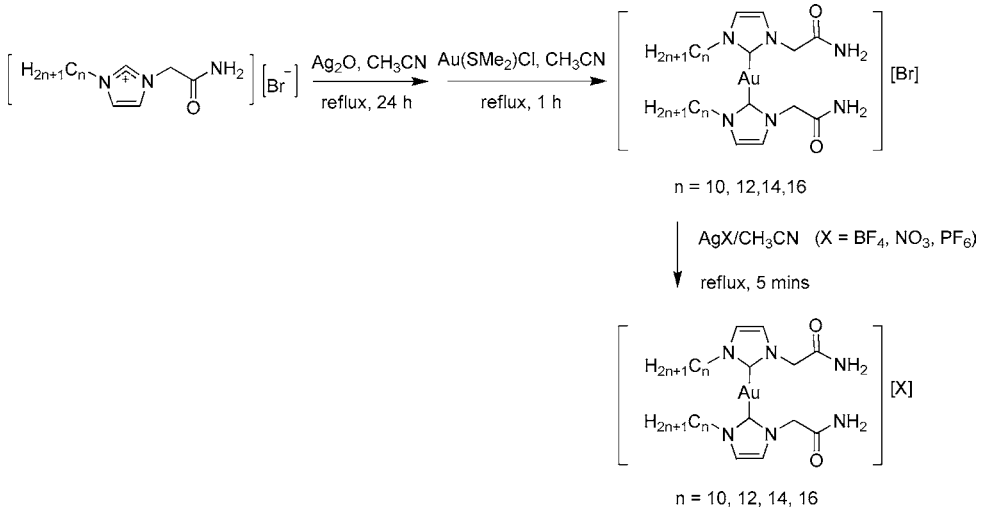

A metallogelator may consist of coordination polymers or discrete metal complexes that form supramolecular assemblies or aggregations. The presence of metal ions could also modify the physical properties of the gels as for MLCs.[59,60,65−67] Therefore metallogels may find applications to a wide range of advanced functional nanoscale materials.

In this work, we report series of silver(I)− and gold(I)−NHCs, in which the NHCs possess one long *N*-alkyl substituent and one *N*-acetamido group. We found that the amide group is an excellent hydrogen bonding motif, which gives a tubular architecture around the metal ions in the solid state. These compounds also assembled to give thermotropic ILCs. Further, the gold(I)−NHC series form metallogels in DMSO at room temperature. Various techniques were employed to better understand the nature of these metallogels. For the first time NMR diffusion ordered spectroscopy (DOSY) was found to be a good tool to study phase transition in gel.

RESULTS AND DISCUSSION

Preparation. In this report acetamido functionalized metal(I)−NHC complexes are abbreviated as $[M(C_n\text{amide-imy})_2][X]$, where $C_n$amide-imy stands for an NHC of imidazol-2-ylidene (denoted as imy) having one N-alkyl substituent (as $C_n = C_nH_{2n+1}$; n = 10, 12, 14, 16, 18, for each series) and one N-acetamido substituent (as amide), while the anion X^- is Br^-, NO_3^-, BF_4^- or PF_6^-, and the M is silver(I) or gold(I) (Scheme 1 and 2). The Ag_2O route was employed to prepare the silver(I)-NHCs. The reaction of Ag_2O with the imidazolium salts 1-(2-amino-2-oxoethyl)-3-(alkyl)-imidazolium bromide in a CH_3CN solution gave the product $[Ag(C_n\text{amide-imy})_2][(AgBr_2)_m/(Br)_{1-m}]$ with mixed $AgBr_2^-$ and Br^- anions. Cationic silver(I)−NHC complexes with mixed $(AgBr_2)^-_m/(Br)^-_{1-m}$ anions have previously been reported.[68−71] The reason for the formation of these mixtures is not clear.[72−74] The salts $[Ag(C_n\text{amide-imy})_2][NO_3]$, $[Ag(C_n\text{amide-imy})_2][PF_6]$ and $[Ag(C_n\text{amide-imy})_2][BF_4]$ were prepared by reaction of the imidazolium salts with Ag_2O, followed by anion metathesis using $AgNO_3$, $AgPF_6$, and $AgBF_4$, respectively. The anion exchange accompanied with the precipitation of AgBr usually complete within 5 min. When necessary, charcoal was added for decolorization.[41] These silver(I) complexes are moderately soluble in CH_3CN, DMSO and DMF, slightly soluble in hot methanol, chlorinated solvents and insoluble in water, diethyl ether and n-hexane.

The gold(I) complexes $[Au(C_n\text{amide-imy})_2][Br]$ (n =10, 12, 14, and 16) were synthesized by utilizing the silver(I)−carbene transfer technique,[75] in which the silver(I)−NHCs prepared in

dx.doi.org/10.1021/ic2011343 | Inorg. Chem. 2012, 51, 98−108

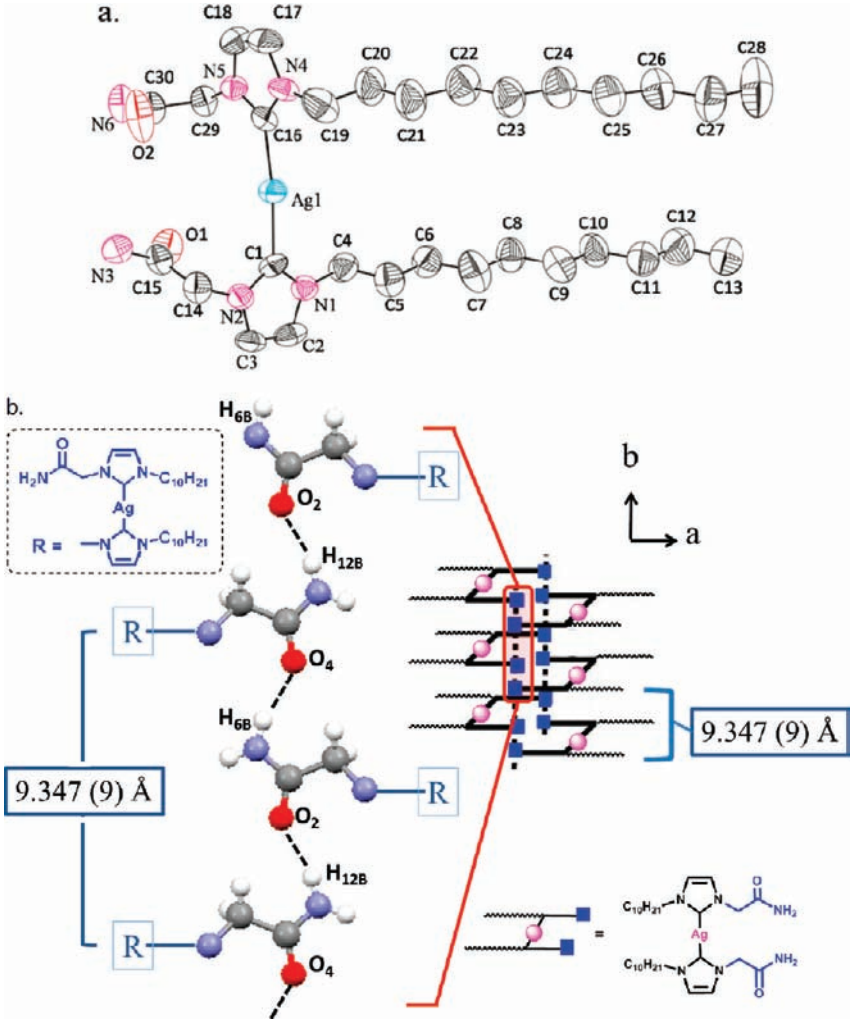

Figure 1. (a) ORTEP diagram of $[Ag(C_{10},amide\text{-}imy)_2][PF_6]$ (50% probability ellipsoids) with partial atomic numbering. Hydrogen atoms and PF_6^- anions are omitted for clarity, and only one of the two independent molecules is shown; (b) an acetamido catemer formed via C═O and NH_2 hydrogen bonding (N−H···O) (left). On the right a schematic drawing for the rectangular shaped architecture constructed through hydrogen bonding shown after.

situ were reacted with $[AuCl(SMe_2)]$. The complete transfer of silver(I) to gold(I) was confirmed by elemental analysis and matrix assisted laser desorption ionization time-of-flight mass spectrometry (MALDI-TOF-MS). Gold(I)−NHC compounds with different anions were obtained through anion metathesis using the corresponding silver salt. These gold(I) complexes are moderately soluble in DMSO and DMF, slightly soluble in hot methanol and CH_3CN, and insoluble in water, chlorinated solvents, diethyl ether, and *n*-hexane. A schematic representation of the synthesis of gold(I)−NHC complexes is given in Scheme 2.

^{13}C NMR signals for the carbenic C^2 carbon of all of the gold(I) complexes and those of the $[Ag(C_n,amide\text{-}imy)_2][(AgBr_2)_m/(Br)_{1-m}]$ complexes appear in the range of 180−185 ppm, typical for the known metal-NHC complexes.[76] For the other silver(I) complexes with NO_3^-, BF_4^-, or PF_6^- anions, signals for the carbene carbons were not observed, presumably due to the fluxional nature of the silver(I)−NHC complexes as has been well recognized. Similar observation and reasoning in other silver(I)−NHC complexes have been noticed.[77−79] Upon complexation, ^1H NMR signals of the imidazole ring for the $C^{4,5}$−H protons and the N−CH_2 protons upfield shift with respect to the NHC precursors.

Assembly of $[Ag(C_{10},amide\text{-}imy)_2][PF_6]$ in Solid State.

A well-formed crystal of $[Ag(C_{10},amide\text{-}imy)_2][PF_6]$ was obtained from a CH_3CN/MeOH solution. This compound crystallizes in the *Cc* space group, and has eight $[Ag(C_{10},amide\text{-}imy)_2]^+$ cations and eight PF_6^- anions in the unit cell with two sets of independent cations. Details of the crystallographic data are given in the Supporting Information (Table S1). An ORTEP drawing of a cation is given in Figure 1a. The two NHC carbenic carbon atoms are linearly coordinated to the silver(I) ion (C−Ag−C = 173.6(3)° and 174.2(3)°) with normal Ag−C bonds (between 2.08(1) and 2.13(1) Å). In the ionic head core, the planes of the two imidazole rings are twisted, with a dihedral angle of 83.42°. The other set of independent cations have a similar structure. This compound adopts a syn conformation with respect to the amido groups, which is different from the "anti" conformation observed for the complexes $[Ag(pym,amide\text{-}imy)_2][PF_6]$ (pym = 2-pyrazinyl) and $[(CH_3,amide\text{-}imy)_2Ag_2Br_2]$,[80,81] in which two amido groups are oppositely located with respect to the silver(I) ions. In the present work, the long alkyl chains lead to the "syn" conformation presumably via favorable hydrophobic interactions. The amido group is an excellent hydrogen bonding motif; rich intermolecular hydrogen bonding inter-

dx.doi.org/10.1021/ic2011343 | *Inorg. Chem.* 2012, 51, 98−108

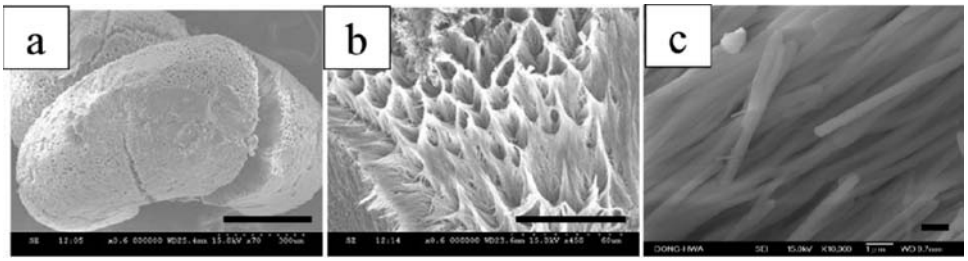

Figure 2. Representative SEM micrographs of solid [Au(C_{12},amide-imy)$_2$][Br] from hot MeOH. (a) porous, donut-shaped feature as seen under low magnification, (b) porous surface for a magnified section and (c) fibrous microstructure under high magnification. (bar = 300, 60, and 1 μm, respectively).

actions between cations are observed. Each of the two syn amido groups associates with oppositely oriented adjacent amides via NH_2···O═C interactions (N−H(12B)···O(2) = 2.020(6) Å and N−H(6B)···O(4) = 2.036(6) Å) (Figure 1b). The assembly through antiparallelly oriented amido groups leads to the formation of an antioriented amido catemer. The separation between two neighboring amido groups of same orientation is 9.347 Å, which is close to the steric requirement for the formation of an antioriented amido catemer as reported.[33] Viewing down along the *b* axis, formation of a rectangular column architecture is observed near the ionic head core (Figure 1b). The PF_6^- anions are located outside the columns and near the silver atoms. Cation−anion interactions are also found as shown in Supporting Information Figure S1, in which the fluorine atoms of the PF_6^- anion interact with the hydrogen atoms of the NH_2, acetamido α-CH, and imidazole ring C−H. Skewed Hg(II) complexes with acetamido functionalized NHCs are also known to assemble to form rectangular column architecture, in which inclusion of solvent molecules in the column occurs.[74] Between neighboring columns, intercolumn interactions via imidazolium rings C_{im}−H and amido O═C (C_{im}−H(18 Å)···O(1) (2.606 Å) and C_{im}−H(47 Å)···O(3) (2.658 Å)) also allow the assembly of columns along the *c* axis (Supporting Information Figure S2). Further hydrophobic alkyl chain−chain interactions between columns along the *a* axis generate the three-dimensional lamellar structure (Supporting Information Figure S3).

Attempts to grow crystals of [Au(C_{12},amide-imy)$_2$][Br] from hot MeOH or CH_3CN gave a porous donut-shaped solid (Figure 2a). Observation under SEM reveals that the solid with sizes of 14−25 mm has an uneven surface (Figure 2b), which is composed of long nanofibers with width of 200−400 nm under high magnification (Figure 2c).

Assembly in Mesophase. Above the melting temperature, these amido functionalized silver(I)− and gold(I)−NHC complexes still assemble to form partially ordered mesophase. The thermal behavior of the assembled silver(I)− and gold(I)−NHC complexes were investigated by thermogravimetric analysis (TGA), polarizing optical microscopy (POM) and differential scanning calorimetry (DSC). The phase transition temperatures and enthalpies are summarized in Tables 1 and 2, respectively.

These silver(I)− and gold(I)−NHC complexes are relatively stable toward heat. Results of TGA show that the gold(I)−NHCs are more stable than the silver(I)−NHCs as expected.[9] The alkyl chain length has a minor influence on the decomposition temperature. The high thermal stability observed in this work reflects the inherent strong gold(I)−NHC and silver(I)−NHC bonds, contrary to popular opinion on organometallic compounds.

Table 1. Phase Transition Behavior of the Silver(I)−NHCs Complexes[a]

Compound	Phase transition
[Ag(C_n,amide-imy)$_2$][BF_4]	
n = 10	Cr ⇌ (170.7 (46.8) / 169.2(37.0)) I
n = 12	Cr ⇌ (172.4(39.5) / 160.2(35.5)) I
n = 14	Cr (171.5(20.6) / 120.3(18.3)) SmA (174.6(1.2) / 171.3(2.1)) I
n = 16	Cr (170.9(15.6) / 117.1(14.3)) SmA (195.3(1.9) / 191.3(1.0)) I
n = 18	Cr (167.2(20.8)) SmA (200) I[d]
[Ag(C_n, amide-imy)$_2$] [NO_3]	
n = 10	Cr (101.0 (39.6) / 82.8 (43.8)) Cr′ (115.8(8.0) / 100.6(11.5)) I
n = 12	Cr (107.2(42.5) / 99.7(15.8)) SmA (153.1(1.9) / 153.4(2.3)) I
n = 14	Cr (110.4(44.2)) SmA (194) I[d]
n = 16	Cr (104.9(42.6)) SmA (200) I[d]
n = 18	Cr (114.2(81.0)) SmA (200) I[d]

[a]The phase transition temperatures (°C) and enthalpies (in parentheses, kJ·mol^{-1}) are determined from the first heating-cooling cycle of DSC thermograms at a scan rate of 10.0 °C·min^{-1} or from POM when partial decomposition occurs. Cr = crystalline phase; Sin A = smectic A phase; I = isotropic phase; d = partial decomposition.

The PF_6^- series of silver(I)− and gold(I)−NHC complexes do not exhibit liquid crystal properties, possibly because of the large size of the anion that leads to weaker Coulombic interactions and fails to sustain the ions undergoing ordered motion. Although, the [Ag(C_n,amide-imy)$_2$][$(AgBr_2)_m$/$(Br)_{1-m}$] series of compounds do assemble to display liquid crystal behavior, their properties were not studied further because of their nonstoichiometric nature.

[Ag(C_n,amide-imy)$_2$][BF_4] compounds with n = 14, 16, or 18 exhibit liquid crystal behavior. A SmA mesophase is tentatively proposed based on the picture observed under POM (Supporting Information Figure S4a), in which fan textures with homeotropically aligned domains are observed. DSC thermograms (the first cycle) for the n = 14, 16, or 18 compounds show that the crystal to mesophase transitions

dx.doi.org/10.1021/ic2011343 | *Inorg. Chem.* 2012, 51, 98−108

Table 2. Phase Transition Behavior of the Gold(I)−NHCs Complexes[a]

Compound	Phase transition
[Au(C_n,amide-imy)$_2$][Br]	
n = 12	Cr 150.6(23.5) / 142.7(9.0) SmA 176.6(2.6) / 172.7(2.5) I
n = 14	Cr 151.1(18.8) / 140.6(7.5) SmA 209.1(2.7) / 205.2(2.3) I
n = 16	Cr 150.7(25.5) / 133.6(18.7) SmA 226.3(1.9) / 221.4(2.0) I
[Au(C_n,amide-imy)$_2$][BF_4]	
n = 10	Cr 175.9(19.4) / 150.5(17.31) I
n = 12	Cr 177.0(8.9) / 148.1(10.1) I
n = 14	Cr 154.5(34.5) / 136.6(31.5) SmA 186.1(3.3) / 183.9(3.1) I
n = 16	Cr 154.8(34.6) / 132.4(29.2) SmA 207.7(2.2) / 204.9(1.9) I
[Au(C_n, amide-imy)$_2$] [NO_3]	
n = 10	Cr 155.3(56.4) / 135.9(51.8) I
n = 12	Cr 154.1(33.3) / 128.2(24.7) SmA 165.7(2.4) / 156.7(1.9) I
n = 14	Cr 153.8(38.7) SmA 210 I[d]
n = 16	Cr 153.4(39.5) SmA 210 I[d]

[a]The phase transition temperatures (°C) and enthalpies (in parentheses, kJ mol^{-1}) are determined from the first heating-cooling cycle of DSC thermograms at a scan rate of 10.0 °C min^{-1} or from POM when partial decomposition occurs. Cr = crystalline phase; SmA = smectic A phase; I = isotropic; d = partial decomposition.

occur at 171.5, 170.9, and 167.2 °C and the clearing processes happen at 174.6, 195.3, and over 200 °C (with decomposition), respectively. The small enthalpy values (<2 kJ·mol^{-1}) observed in the clearing process, are consistent with a partially ordered state in the mesophase. Cooling processes for the compounds with n = 14 and 16 from isotropic to mesophase occur at 171.3 and 191.3 °C, while the freezing processes were observed at 120.3 and 117.1 °C, respectively. For each reversible process, a lower phase transition temperature is often observed in the cooling than in the heating process, a phenomenon with supercooling. Compounds [Ag(C_n,amide-imy)$_2$][NO_3] of n = 12, 14, 16, or 18 are also SmA liquid crystals, which display melting processes between 105 and 114 °C, and clearing processes from 153 up to ∼200 °C, partial decompositions were observed for the latter three compounds.

Partially ordered assembly of the [Au(C_n,amide-imy)$_2$][Br] series at mesophase are observed for n = 12, 14, and 16. DSC thermograms reveal that the melting points are around 151 °C for all the chain lengths of n = 12, 14, or 16; but the clearing temperatures increase upon increasing the chain length: 176.6, 209.1, or 226.3 °C for n = 12, 14 or 16, respectively. This observation suggests that the hydrophobic chain−chain interactions dominate the clearing but not the melting process. Observation under POM (Supporting Information Figure S4b) suggests an SmA phase for these bromide salts. The series of [Au(C_n,amide-imy)$_2$][BF_4] compounds exhibit liquid crystal behavior for the compounds with n = 14 and 16, but not 10 and 12. All of them also exhibit an SmA mesophase. The DSC thermograms (the first cycle) for the compounds with n = 14 and 16 show that the melting temperatures are at 154.5 and 154.8 °C, and the clearing temperatures appear at 186.1 and 207.7 °C, respectively. Similar to the bromide series, the chain length affects the clearing but not the melting process. In the [Au(C_n,amide-imy)$_2$][NO_3] series, the compound with n = 10 is nonmesomorphic, while the compounds with n = 12, 14, or 16 show liquid crystal behavior in the range of 154.1−165.7 °C, 153.8−210.0 °C, and 153.4−210.0 °C, respectively. The clearing processes for the compounds with n = 14 and 16 occur accompanied by decomposition. Textures observed under POM also suggest an SmA mesophase for the NO_3^- series.

A careful examination of the thermal behaviors of the silver(I)− and gold(I)−NHC complexes, reveals that for each series of mesomorphic compounds, a striking similarity in the melting temperatures is observed despite the difference in chain length, whereas there is an increase in the clearing temperatures upon increasing the chain length, except those instances accompanied by partial decomposition. Furthermore, melting temperatures of the mesomorphic gold(I)−NHC compounds are insensitive even to the difference in anions: ∼151 °C for the Br^- series, ∼155 °C for the BF_4^- series, and ∼154 °C for the NO_3^- series. The minimum influence of different anions on the melting temperature is possibly due to the strong amido hydrogen bonding interactions between cations in the rigid framework; these interactons provide a large lattice energy, which overrides the cation−anion interactions. That is, the strong amido hydrogen bonding interactions are the dominating factor in the melting processes of these amido-functionalized compounds.

Temperature-dependent PXRD experiments were utilized to further understand the order of assembly in the solid and mesophase. Diffractograms for all the solid samples show a set of equally spaced reflections in the small angle region, characteristic for lamellar structures, in which a layer distance could be obtained from the corresponding (001) reflection. All the compounds in mesophase exhibit a strong (001) reflection sometimes followed by a weak (002) reflection at the small angle region and a faint halo at the middle angle region of ∼2θ = 18°. A typical diffractogram for a silver(I)−NHC compound showing the pattern at mesophase is given in Figure 3, whereas

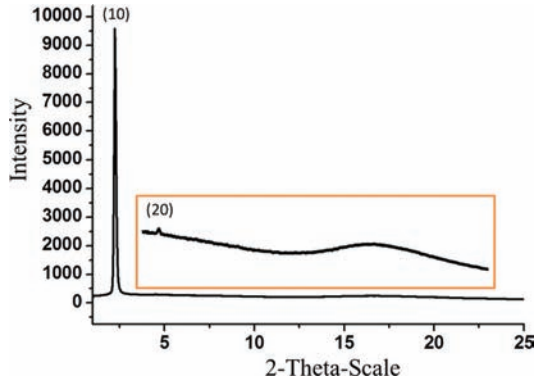

Figure 3. XRD pattern of [Ag(C_{14},amide-imy)$_2$][NO_3] at 140 °C in mesophase.

dx.doi.org/10.1021/ic2011343 | Inorg. Chem. 2012, 51, 98−108

typical diffractograms for each series of silver(I)− and gold(I)−NHCs are shown in Supporting Information Figure S5. Layer spacings for all the silver(I)-NHCs in the solid state and mesophase are provided in Supporting Information Table S2. $[Ag(C_{12},amide\text{-}imy)_2][NO_3]$ as an example will be discussed first. This compound has a layer distance of 26.5 Å at room temperature (crystalline phase). If one compares this value with the 24.5 Å observed from the single crystal structure of $[Ag(C_{10},amide\text{-}imy)_2][PF_6]$, a similar interdigitated bilayeral structure is proposed for the NO_3^- salt. Upon increasing the temperature to 120 °C for the NO_3^- salt in the mesophase, the diffraction pattern exhibits a (001) reflection corresponding to a layer distance of 31.4 Å. The longer *d*-spacing observed in the mesophase than that in solid is presumably due to a structural change from highly interdigitated alkyl chains to none or partially interdigitated chains. In the mesophase, the layer spacings at 120, 130, and 140 °C are 31.4, 31.2, and 30.7 Å, respectively. The behavior of decreasing *d*-spacing with increasing temperature in the mesophase is consistent with an SmA mesophase, which has a molecular rod perpendicular to the layer plane such that increasing the temperature would increase the thermal motion of the chains and thus decrease the layer distance. For the compounds with n = 14, 16, or 18, the layer spacings in the crystalline and mesophases increase along with an increase in the chain length. The corresponding values are 30.7, 32.7, and 36.0 Å in the crystalline phase, and 33.4, 37.1, and 39.7 Å at mesophase. Similar results are observed for the BF_4^- salts. As a comparison, the layer distances for the compounds with n = 14, 16, and 18 are 29.4, 33.2, and 36.1 Å in the crystaline phase, and 32.9, 33.8, and 36.9 Å at mesophase, respectively.

PXRD data for the layer distances of gold(I)−NHC series are given in Supporting Information Table S3. For the $[Au(C_n,amide\text{-}imy)_2][Br]$ compounds with n = 12, 14, or 16, the corresponding *d* values are 28.9, 31.6, and 32.4 Å in the crystalline phase, and 30.0, 33.4, and 35.1 Å, at mesophase. The $[Au(C_n,amide\text{-}imy)_2][BF_4]$ compounds with n = 14 and 16, show *d*-spacing values of 30.7 and 32.2 Å in the crystalline phase and 32.7 and 35.3 Å at the mesophase, respectively. Finally for the $[Au(C_n,amide\text{-}imy)_2][NO_3]$ compounds with n = 12, 14, and 16, the *d*-spacing values are 27.2, 29.4, and 32.4 Å at the crystal phase, and 31.0, 33.3, and 36.1 Å, at the mesophase, respectively. Since the layer spacings for the silver(I)− and gold(I)−NHC compounds with similar chain lengths and anions in the solid have relatively close values, similar solid structures are proposed; so are the mesophase structures.

Assembly in DMSO. Gold(I)−NHCs in DMSO form gels of well-order assembly (Figure 4a). The compound $[Au(C_{16},amide\text{-}imy)_2][NO_3]$ illustrates this behavior. The gel was prepared by heating a solution of 1.0 wt % of the $[Au(C_{16},amide\text{-}imy)_2][NO_3]$ in DMSO to 70 °C to give a clear solution, which was then allowed to rest for 3 h to completely convert the sol to a gel form. The formation of gel was evaluated by the "sample vial inversion" method. Between the concentrations of 1.0 and 5.8 wt % in DMSO, the gel is stable toward inversion of an NMR sample tube for more than two weeks, and gel-to-sol phase transition occurs upon increasing the temperature to ~45 °C. The thermal behavior of the gel was studied by DSC. A broad endothermic peak between 36 and 45 °C with ΔH = 1.5 $J \cdot g^{-1}$ in the heating process is found (Figure 4b). A diffractogram of the gel shows a sharp (001) and several weak (00*n*) reflections followed by a large broad band (2θ = 17.4°) (Figure 4c). Again a lamellar structure at layer distance of 39.4 Å, and a liquid-like chain−chain distance of ~4.4 Å are found.

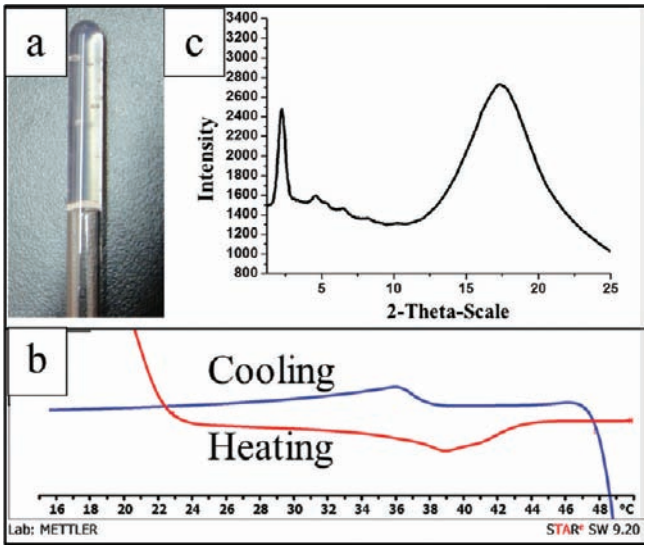

Figure 4. (a) Inverted NMR tube for the gel of $[Au(C_{16},amide\text{-}imy)_2][NO_3]$ in DMSO (1.0 wt %); (b) DSC thermograms of $[Au(C_{16},amide\text{-}imy)_2][NO_3]$ at 4.2 wt % in DMSO; (c) room temperature X-ray diffraction patterns of 4.2 wt % $[Au(C_{16},amide\text{-}imy)_2][NO_3]$ in DMSO.

Morphology of the gelator (xerogel) was examined by electron microscopies. Samples of xerogels were produced by heating the gels at 100 °C for 4 h in a fumehood; the residues were then mounted for SEM experiments. For TEM experiments, the samples were prepared by dropping the DMSO solution on carbon-coated copper grids. Representative images of SEM and TEM for some xerogels of gold(I)−NHCs are shown in Figure 5. The major morphology observed is densely populated fibers mostly with diameters of 100−150 nm (Figure 5a), they sometimes bundle together to form belts (Figure 5b and c). There are also some hollow oriental lantern-shaped structures with diameters of 3−10 μm constructured from belt-like fibrous bundles (Figure 5a, c, d, and e). Occasionally, helical belts are seen (Figure 5f). The diverse morphologies observed from this gel are likely caused by the rich hydrogen bonding, hydrophobic, and Coulombic interactions provided by the gold(I)−NHCs. Gold(I) ion is essential for this behavior; since it provides two amido and two long alkyl groups in a cation, whereas the NHC precursor, an amido functionalized imidazolium salt, which has only one amido and alkyl groups, does not form any gel and xerogel.

The technique of DOSY NMR with a pulsed gradient has been employed to study the molecular assembly behavior in solution.[82] The concentration dependent diffusion coefficient of the molecules is related to the absolute temperature T, the viscosity of the solvent η and the hydrodynamic radius of the solute R_h according to the Stokes−Einstein equation (eq 1).[83] When aggregation behavior appears, changing the concentration will yield different D and R_h values. A similar technique has also been used to examine the diffusion coefficients of lithium doped liquid crystalline material with changing temperature. A turning point in the plot of log D vs T was found to correspond to the phase transition (clearing temperature) of that material.[84] In this work, we utilized variable temperature NMR DOSY to study the phase transition

dx.doi.org/10.1021/ic2011343 | *Inorg. Chem.* 2012, 51, 98−108

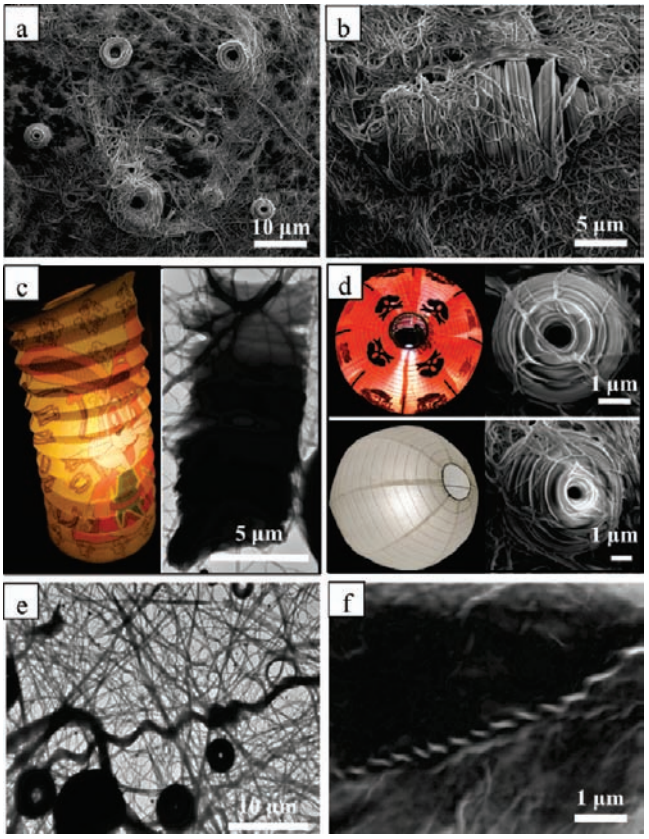

Figure 5. (a and b) are representative SEM micrographs of the xerogel of $[Au(C_{12},amide\text{-}imy)_2][NO_3]$ from DMSO; (c) a TEM image of the xerogel showing a lantern-shaped morphology, picture of the latern www.flickr.com/photos/40734231@N00/3151093750/; (d) SEM images of lantern-shaped fibrous bundles of xerogel; (e) the TEM image of fibers, lantern-shaped fibrous bundles and a helical like belt; (f) SEM image of the xerogel from $[Au(C_{18},amide\text{-}imy)_2][NO_3]$ showing a helical belt.

of a gold(I)−NHC gel. Although the terms η and R_h in eq1 are also temperature dependent,[85,86] the influence is small when no phase transition occurs. This is especially true for a sample studied in a small temperature range.

$$D = kT/6\pi\eta R_h \quad (1)$$

where D = diffusion coefficient (m^2 s^{-1}), k = Boltzmann constant (m^2 kg s^{-2} K^{-1}), T = the absolute temperature (K), η = viscosity of solvent (kg s^{-1} m^{-1}), and R_h = hydrodynamic radius (m).

The result of ploting log D vs T is shown in Figure 6. The log D value for the gel at the concentration of 2.9 wt % increases gradually from −9.71 at 298.0 K to −9.48 at 318.0 K. Then, at the temperature of 320.5 K, there is a slightly greater increment of log D (−9.42). Upon further heating the sample to 323.0 K, a dramatic increase in the log D value (−8.98) is observed. In other words, there is a greater change of log D per K beyond 318.0 K, at which, a phase transition from gel to solution takes place. No further increase in the temperature could be performed as a result of the limitation of our instrument. For the gel at a higher concentration (3.5 wt %), similar results of temperature-dependent diffusion coefficient were also observed. For comparison, the solution of gold(I)−NHC in d_6-DMSO (0.9 wt %) was also studied; a rather smooth increment of log D from −9.65 to −8.79 is observed upon raising the

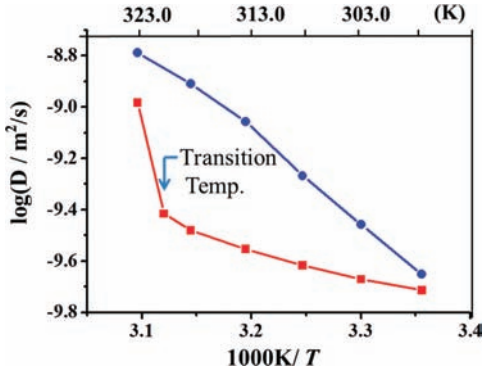

Figure 6. Temperature dependence of the diffusion coefficient of the $[Au(C_{16},amide\text{-}imy)_2][NO_3]$ in DMSO (a) solution at 0.9 wt % (●); (b) gel at 2.9 wt % (■).

temperature from 298.0 to 323.0 K. Results from this work indicate that in solution the progression of log D against T is almost linear between 298.0 and 318.0 K; in gel, however, a phase transition can cause a dramatic change of viscosity η and log D. This observations support the assumption that when no phase transition occurs and the concentration is not changed in the solution or gel state, the temperature has minimum effect on the viscosity of the solution and the hydrodynamic radius of the solute. This technique is useful for the study of the phase transition from gel to solution.

We notice that for $[Au(NHC)_2][anion]$ type compounds, when the *N*-substituents are simple alkyl chain, no gel property is observed. Therefore, amido group in these gold(I)−NHC compounds apparently plays a critical role in the formation of gel. IR spectroscopy was therefore employed to study the behavior of amido group in the gelation process. The investigation of hydrogen bonding interactions between the solvent DMSO and amido group from nicotinamide has been carried out, and C═O···H_3CS and NH_2···O═S hydrogen bonds are proposed.[87] For our system, IR spectrum of the solid $[Au(C_{16},amide\text{-}imy)_2][NO_3]$ shows a carbonyl stretching band at 1681 cm^{-1}, and asymmetric and symmetric N−H stretching bands at 3373 and 3163 cm^{-1}, respectively (Figure 7a). In

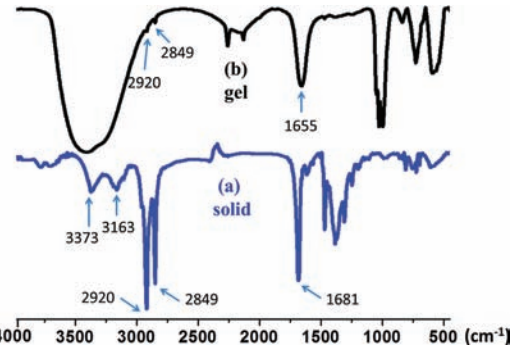

Figure 7. FTIR spectra of $[Au(C_{16},amide\text{-}imy)_2]$ $[NO_3]$ (a) solid state and (b) gel state in DMSO (3.5 wt %).

DMSO gel, the carbonyl band shifts to 1655 cm^{-1}, and the NH_2 vibration appears as a broad band at ∼3400 cm^{-1}. The lower C═O stretching frequency indicates its interaction with the CH_3 protons in DMSO. The broad NH_2 band is presumably caused by the nondirectional hydrogen bonding interactions among NH_2, O═S, and O−H groups. Variable-

dx.doi.org/10.1021/ic2011343 | *Inorg. Chem.* 2012, 51, 98−108

temperature ^{1}H NMR spectroscopy was also utilized to follow the chemical shifts of the NH_2 groups in the gel. [Au(C_{16},amide-imy)$_2$][NO_3] in d_6-DMSO shows a gradual upfield shift of the NH_2 proton signals from 298 K at 7.63 and 7.33 ppm to 323 K at 7.54 and 7.20 ppm, respectively (Supporting Information Figure S6). The change of chemical shift of the amido NH_2 group upon raising the temperature could be attributed to its participation in the formation of gel as has been similarly discussed for the gels of dicarboxamide compounds in $CDCl_3$.[88]

Interestingly, both the solid and gel samples exhibit a set of identical C−H stretching frequencies at 2920 and 2849 cm^{-1}, which are compared to the 2920 and 2850 cm^{-1} values observed for those *n*-alkanes[89] in the solid state and 2920 and 2851 cm^{-1} for phospholipids in gel state.[90] Note that the C−H stretching bands for [Au(C_{16},amide-imy)$_2$][NO_3] in the mesophase are at 2926 and 2854 cm^{-1} (Supporting Information Figure S7). These values are close to the values of 2928 and 2856 cm^{-1} observed for liquid *n*-alkanes.[86] Thus results of the C−H stretching data suggest that the order of chain motion in the solid and gel states are comparable, whereas the order of the alkyl chains in the mesophase is more liquid-like, as true for a liquid crystalline material. The C−H stretching vibration of methylene group has been used to monitor the process of gelation for octadecyltrimethoxysilane.[91]

Other gold(I)−NHCs with Br^- and BF_4^- anions also form gels in DMSO; among these, the NO_3^- and Br^- gels are relatively more stable than the gels of the BF_4^- salt. Presumably the ability to provide a better cation−anion interaction and a better solvation for the smaller Br^- and NO_3^- anions than BF_4^- might cause a more stable gel. It is rather surprising to note that for the two seemingly similar series of silver(I) and gold(I) compounds, only the gold(I) compounds exhibit gelation properties. At present, we have no better explanation other than that the silver(I) complexes are labile in solution, thus destabilizing the gel formation. Indeed, the absence of ^{13}C−^{107}Ag and ^{13}C−^{109}Ag couplings in the ^{13}C NMR spectra of these silver(I)−NHC compounds evidently supports their lability.

CONCLUSION

Silver(I) and gold(I) complexes of NHCs with acetamido and long alkyl chain functionalization could self-assemble in the solid state through Coulombic, hydrophobic, and especially amido hydrogen bonding interactions to give a lamellar structure with tubular architecture around the ionic head core. Self-assembly of these functionalized NHC complexes also leads to the formation of the first example of thermotropic silver(I)−NHCs, and the first example of gel of gold(I)−NHCs. Gold(I) ion is crucial for the formation of gels; without gold(I) ion, amido functionalized imidalium salts themselves do not form gel. Aggregation of the gold(I)−NHCs also give a xerogel of long wires, oriental lantern-shaped bundles of belts and helical belts. Results from an IR study show that the degree of alkyl chain motion in the gel state is smaller than that in the mesophase, yet comparable to that in the solid state. Furthermore, an NMR DOSY study indicates that the diffusion coefficient of the gel increases slowly upon raising the temperature until reaching the point where phase transition from gel to isotropic liquid occurs, after which, there is a dramatic change of the diffusion coefficient, and thus a good tool to study the thermal behavior of gels.

MATERIALS AND METHODS

All the reactions were carried out in air. The solvents and regents were purchased from Aldrich Acros and used as received. NMR spectra were recorded on a Bruker AC-F300 spectrometer (^{1}H, 300 MHz; ^{13}C, 75 MHz). Chemical shifts are given in ppm in d_6-DMSO with tetramethysilane, $Si(CH_3)_4$ as an internal standard. The diffusion NMR experiment was acquired on a BRUKER 600 UltraShield equipped with a 5 mm BBO inverseprobe. Mass analyses were performed using a Bruker Autoflex MALDI-TOF mass spectrometer. IR spectra were recorded with a Perkin-Elmer Spectrum One. Elemental microanalyses were performed by the Taiwan Instrumentation Center. Optical characterization was performed on an Olympus BH-2 polarizing microscope equipped with a Mettler FP 82 hot stage and a Mettler FP 90 central processor. Differential scanning calorimetry (DSC) was performed by using a Perkin-Elmer DSC-10 calorimeter under flowing N_2. Thermogravimetric analysis (TGA) was performed using a Perkin-Elmer model 10 instrument. The powder X-ray diffraction data was collected by National Dong Hwa University with Cu K_α radiation (XRD D8 Advanced, Brüker) and by National Synchrotron Radiation Research Center (NSRRC). The dynamic light scattering (DLS) was performed by using a ZEN3600. Transmission electron microscopy (TEM), JEOL JEM-3010 FE-TEM, was operated at 120 kV. Scanning electron microscopy (SEM) images were obtained using a JEOL JEM-7000F operated at 3 kV.

Synthesis of [Ag(C_{10},amide-imy)$_2$][NO_3]. A mixture of [C_{10},amide-im][Br] (0.5 g, 1.44 mmol) and silver oxide (0.22 g, 0.94 mmol) was refluxed in CH_3CN (65 mL) for 1 day in dark. $AgNO_3$ (0.123 g, 0.73 mmol) was then added and reacted for 5 min, during which a white precipitate was observed. The solution was filtered and the filtrate was collected. The solvent was then removed using a rotary evaporator. The white crude product was treated with charcoal in CH_3CN at 60 °C until the mixture became a clear solution then recrystallized from CH_3CN/ether to afford snow-white crystalline product (303 mg, 60% yield). ^{1}H NMR (300 MHz, d_6-DMSO, 298 K): δ = 7.65 (s, 2H, NH_2), 7.46 (s, 2H, CH_{aromat}), 7.40 (s, 2H, CH_{aromat}), 7.32 (s, 2H, NH_2), 4.76 (s, 4H, CH_2−CO), 4.08 (t, ^3J (H,H) = 7 Hz, 4H, α-CH_2), 1.74 (m, 4H, β-CH_2), 1.19 (m, 28H, CH_2), 0.82 (t, ^3J (H,H) = 7 Hz, 6H, CH_3); elemental analysis calcd (%) for $C_{30}N_7H_{54}O_5Ag\cdot H_2O$: C 50.14, H 7.85, N 13.64; found: C 50.15, H 7.73, N 13.54.

Synthesis of [Ag(C_{10},amide-imy)$_2$][PF_6]. A mixture of [C_{10},amide-im][Br] (0.5 g, 1.44 mmol) and silver oxide (0.22 g, 0.94 mmol) was refluxed in CH_3CN (65 mL) for 1 day in dark. $AgPF_6$ (0.185 g, 0.73 mmol) was then added. The other procedures and workup were similar to those for the NO_3^- salt to afford snow-white crystalline product (314 mg, 60% yield). ^{1}H NMR (300 MHz, d_6-DMSO, 298 K): δ = 7.64 (s, 2H, NH_2), 7.46 (s, 2H, CH_{aromat}), 7.39 (s, 2H, CH_{aromat}), 7.31 (s, 2H, NH_2), 4.77 (s, 4H, CH_2−CO), 4.10 (t, ^3J (H,H) = 7 Hz, 4H, α-CH_2), 1.75 (m, 4H, β-CH_2), 1.19 (m, 28H, CH_2), 0.83 (t, ^3J (H,H) = 7 Hz, 6H, CH_3); elemental analysis calcd (%) for $C_{30}N_6H_{54}O_2AgPF_6$: C 45.98, H 6.95, N 10.72; found: C 46.27, H 6.97, N 10.44.

Synthesis of [Ag(C_{10},amide-imy)$_2$][BF_4]. A mixture of [C_{10},amide-im][Br] (0.5 g, 1.44 mmol) and silver oxide (0.22 g, 0.94 mmol) was refluxed in CH_3CN (65 mL) for 1 day in dark. $AgBF_4$ (0.143 g, 0.73 mmol) was then added. The snow-white crystalline product (314 mg, 60% yield) was obtained after workup procedures similar to those for the NO_3^- salt. ^{1}H NMR (300 MHz, d_6-DMSO, 298 K): δ = 7.66 (s, 2H, NH_2), 7.46 (s, 2H, CH_{aromat}), 7.39 (s, 2H, CH_{aromat}), 7.34 (s, 2H, NH_2), 4.77 (s, 4H, CH_2−CO), 4.10 (t, ^3J (H,H) = 7 Hz, 4H, α-CH_2), 1.75 (m, 4H, β-CH_2), 1.21(m, 28H, CH_2), 0.82 (t, ^3J (H,H) = 7 Hz, 6H, CH_3); elemental analysis calcd (%) for $C_{30}N_6H_{54}O_2AgBF_4\cdot 0.5\ H_2O$: C 49.09, H 7.55, N 11.44; found: C 49.29, H 7.67, N 11.40.

Synthesis of [Au(C_{12},amide-imy)$_2$][Br]. A mixture of [C_{12},amide-imy][Br] (0.5 g, 1.34 mmol) and silver oxide (0.20 g, 0.87 mmol) was refluxed in CH_3CN (65 mL) for 1 day in dark. Au(SMe_2)Cl (0.21 g, 0.74 mmol) was added to the reaction mixture and was allowed to react under reflux condition for 60 min. The

dx.doi.org/10.1021/ic2011343 | Inorg. Chem. 2012, 51, 98−108

solution was filtered hot to remove the precipitate and the solvent was removed using a rotary evaporator. The white residue obtained was then washed several times with methanol and diethyl ether and recrystallized from CH_3CN/ether to afford snow-white crystalline product. The solvent was removed using a rotary evaporator. The white residue obtained was then washed several times with methanol and diethyl ether and recrystallized from CH_3CN/ether to afford the snow-white crystalline title compound (394 mg, 68%); ^{1}H NMR (300 MHz, d_6-DMSO, 298 K): δ = 7.82 (s, 2H, NH_2), 7.52 (s, 2H, CH_{aromat}), 7.45 (s, 2H, CH_{aromat}), 7.34 (s, 2H, NH_2), 4.85 (s, 4H, CH_2−CO), 4.16 (t, ^3J (H,H) = 7 Hz, 4H, α-CH_2), 1.79 (m, 4H, β-CH_2), 1.19 (m, 36H, CH_2), 0.83 (t, ^3J (H,H) = 7 Hz, 6H, CH_3); MS: m/z (%): 783.254 (100) [[Au(C_{12},amide-imy)$_2$]$^+$]; elemental analysis calcd (%) for $C_{34}N_6H_{62}O_2AuBr$: C 47.28, H 7.23, N 9.73; found: C 47.05, H 7.56, N 9.76.

Synthesis of [Au(C_{10},amide-imy)$_2$][BF_4]. A mixture of [C_{10},amide-imy][Br] (0.5 g, 1.44 mmol) and silver oxide (0.22 g, 0.94 mmol) was refluxed in CH_3CN (65 mL) for 1 day in dark. Au(SMe_2)Cl (0.25 g, 0.87 mmol) was added to the reaction mixture and was allowed to react under reflux condition for 60 min. The solution was filtered hot to remove the precipitate. $AgBF_4$ (0.143 g, 0.73 mmol) was added to this hot filtrate, and was allowed to reaction for 5 min under reflux. The solution was again filtered to remove the precipitate. The solvent was then removed using a rotary evaporator. The white residue obtained was then washed several times with methanol and diethyl ether and recrystallized from CH_3CN/ether to afford snow-white crystalline product (235 mg, 40% yield). ^{1}H NMR (300 MHz, d_6-DMSO, 298 K): δ = 7.66 (s, 2H, NH_2), 7.46 (s, 2H, CH_{aromat}), 7.39 (s, 2H, CH_{aromat}), 7.34 (s, 2H, NH_2), 4.77 (s, 4H, CH_2−CO), 4.10 (t, ^3J (H,H) = 7 Hz, 4H, α-CH_2), 1.75 (m, 4H, β-CH_2), 1.19(m, 28H, CH_2), 0.82 (t, ^3J (H,H) = 7 Hz, 6H, CH_3); elemental analysis calcd (%) for $C_{30}N_6H_{54}O_2AuBF_4 \cdot 0.5\ H_2O$: C 43.75, H 6.73, N 10.20; found: C 43.84, H 6.67, N 10.14.

Synthesis of [Au(C_{10},amide-imy)$_2$][PF_6]. A mixture of [C_{10},amide-imy][Br] (0.5 g, 1.44 mmol) and silver oxide (0.22 g, 0.94 mmol) was refluxed in CH_3CN (65 mL) for 1 day in dark. Au(SMe_2)Cl (0.25 g, 0.87 mmol) was added to the reaction mixture and was allowed to react under reflux condition for 60 min. The solution was filtered hot to remove the precipitate. $AgPF_6$ (0.185 g, 0.73 mmol) was added to this hot filtrate. Procedures similar to those for [Au(C_{10},amide-imy)$_2$][BF_4] were followed to afford snow-white crystalline product (235 mg, 40% yield). ^{1}H NMR (300 MHz, d_6-DMSO, 298 K): δ = 7.66 (s, 2H, NH_2), 7.52 (s, 2H, CH_{aromat}), 7.44 (s, 2H, CH_{aromat}), 7.35 (s, 2H, NH_2), 4.82 (s, 4H, CH_2−CO), 4.16 (t, ^3J (H,H) = 7 Hz,4H, α-CH_2), 1.79 (m, 4H, β-CH_2), 1.19 (m, 28H, CH_2), 0.83 (t, ^3J (H,H) = 7 Hz,6H, CH_3); elemental analysis calcd (%) for $C_{30}N_6H_{54}O_2AuPF_6 \cdot H_2O$: C 40.45, H 6.34, N 9.43; found: C 40.52, H 6.26, N 9.28.

Synthesis of [Au(C_{10},amide-imy)$_2$][NO_3]. A mixture of [C_{10},amide-imy][Br] (0.5 g, 1.44 mmol) and silver oxide (0.22 g, 0.94 mmol) was refluxed in CH_3CN (65 mL) for 1 day in dark. Au(SMe_2)Cl (0.25 g, 0.87 mmol) was added to the reaction mixture and was allowed to react under reflux condition for 60 min. The solution was filtered hot to remove the precipitate. $AgNO_3$ (0.123 g, 0.73 mmol) was added to this hot filtrate. Procedures similar to those for [Au(C_{10},amide-imy)$_2$][BF_4] were then followed to afford snow-white crystalline product (235 mg, 40% yield). ^{1}H NMR (300 MHz, d_6-DMSO, 298 K): δ = 7.66 (s, 2H, NH_2), 7.53 (s, 2H, CH_{aromat}), 7.45 (s, 2H, CH_{aromat}), 7.35 (s, 2H, NH_2), 4.82 (s, 4H, CH_2−CO), 4.16 (t, ^3J (H,H) = 7 Hz, 4H, α-CH_2), 1.80 (m, 4H, β-CH_2), 1.20 (m, 28H, CH_2), 0.83 (t, ^3J (H,H) = 7 Hz, 6H, CH_3); elemental analysis calcd (%) for $C_{30}N_7H_{54}O_5Au \cdot H_2O$: C 44.61, H 6.99, N 12.14; found: C 44.33, H 7.00, N 12.02.

X-ray Structure Determination. The single crystal X-ray data were collected on a Bruker SMART diffractometer equipped with a CCD array detector with a graphite monochromator using Mo Kα radiation (k = 0.71073 Å) in Φ and ω scan modes. The structure of [Ag(C_{10},amide-imy)$_2$][PF_6] was solved by the heavy atom method. For H-atoms a riding model was employed. Crystallographic data for the structural analysis has been deposited to the Cambridge Crystallographic Data Center (CCDC) with the number of 809547 is obtained. Details of crystal parameters, data collection and structure refinements were summarized in Supporting Information Table S1.

Microscopic Observations. Sample for the SEM and TEM experiments, were prepared by drying a piece of gel at 100 °C for 4 h in a fumehood.

■ ASSOCIATED CONTENT

Supporting Information

X-ray crystallographic data for [Ag(C_{10},amide-imy)$_2$][PF_6] in CIF format, experimental section for other Ag(I)−NHC and Au(I)−NHC complexes, single crystal data for [Ag(C_{10},amide-imy)$_2$][PF_6] (Table S1), cation−anion interactions of [Ag(C_{10},amide-imy)$_2$][PF_6] (Figure S1), schematic drawing of [Ag(C_{10},amide-imy)$_2$][PF_6] (Figure S2), chain−chain interactions of [Ag(C_{10},amide-imy)$_2$][PF_6] (Figure S3), POM images of Ag(I)−NHC and Au(I)−NHC complexes (Figure S4), XRD pattern of Ag(I)−NHC and Au(I)−NHC complexes (Figure S5), layer d-spacings of the silver(I)−NHC complexes (Table S2), layer d-spacings of the gold(I)−NHC complexes (Table S3), variable-temperature ^{1}H NMR spectra for the gel (Figure S6), and FTIR spectra of [Au(C_{16},amide-imy)$_2$][NO_3] at mesophase (180 °C) (Figure S7). This material is available free of charge via the Internet at http://pubs.acs.org.

■ AUTHOR INFORMATION

Corresponding Author

*E-mail: ijblin@mail.ndhu.edu.tw. Tel: +886-3-863-3599. Fax: +886-3-863-3570.

■ ACKNOWLEDGMENTS

We gratefully acknowledge the National Science Council (NSC) of Taiwan for financial support. We thank the National Synchrotron Radiation Research Center of Taiwan and National Dong Hwa University Nanotechnology Research Center (NSC 98-2120-M-259-002) for providing research facilities. We appreciate the help of Prof. M. V. Baker in assisting in the preparation of this manuscript and Jung-Tang Lu for measuring in the NMR DOSY studies.

■ REFERENCES

(1) Jones, W. D. *J. Am. Chem. Soc.* **2009**, *131*, 15075−15077.
(2) Kascatan-Nebioglu, A.; Panzner, M. J.; Tessier, C. A.; Cannon, C. L.; Youngs, W. J. *Coord. Chem. Rev.* **2007**, *251*, 884−895.
(3) Berlin, J. M.; Grubbs, R. H. *Organometallics* **2010**, *29*, 403−408.
(4) Garrison, J. C.; Youngs, W. J. *Chem. Rev.* **2005**, *105*, 3978−4008.
(5) Lee, C. K.; Lee, K. M.; Lin, I. J. B. *Organometallics* **2002**, *21*, 10−12.
(6) Lin, I. J. B.; Vasam, C. S. *Coord. Chem. Rev.* **2007**, *251*, 642−670.
(7) Samantaray, M. K.; Pang, K.; Shaikh, M. M.; Ghosh, P. *Inorg. Chem.* **2008**, *47*, 4153−4165.
(8) Bourissou, D.; Guerret, O.; Gabbaï, F. P.; Bertrand, G. *Chem. Rev.* **2000**, *100*, 39−91.
(9) Boehme, C.; Frenking, G. *Organometallics* **1998**, *17*, 5801−5809.
(10) Ray, S.; Mohan, R.; Singh, J. K.; Samantaray, M. K.; Shaikh, M. M.; Panda, D.; Ghosh, P. *J. Am. Chem. Soc.* **2007**, *129*, 15042−15053.
(11) Jang, H.; Zhugralin, A. R.; Lee, Y.; Hoveyda, A. H. *J. Am. Chem. Soc.* **2011**, *133*, 7859−7871.
(12) Wang, H. M. J.; Vasam, C. S.; Tsai, T. Y. R.; Chen, S. H.; Chang, A. H. H.; Lin, I. J. B. *Organometallics* **2005**, *24*, 486−493.
(13) Barnard, P. J.; Wedlock, L. E.; Baker, M. V.; Berners-Price, S. J.; Joyce, D. A.; Skelton, B. W.; Steer, J. H. *Angew. Chem., Int. Ed.* **2006**, *45*, 5966−5970.

(14) Hickey, J. L.; Ruhayel, R. A.; Barnard, P. J.; Baker, M. V.; Berners-Price, S. J.; Filipovska, A. *J. Am. Chem. Soc.* **2008**, *130*, 12570–12571.
(15) Peris, E. *Top. Organomet. Chem.* **2007**, *21*, 83–116.
(16) Brake, J. M.; Daschner, M. K.; Luk, Y.-Y.; Abbott, N. L. *Science* **2003**, *302*, 2094–2097.
(17) Armand, M.; Endres, F.; MacFarlane, D. R.; Ohno, H.; Scrosati, B. *Nat. Mater.* **2009**, *8*, 621–629.
(18) Ichikawa, T.; Yoshio, M.; Hamasaki.; Kagimoto, A.; J.; Ohno, H.; Kato, T. *J. Am. Chem. Soc.* **2011**, *133*, 2163–2169.
(19) Arias, J.; Bardají, M.; Espinet, P.; Folcia, C. L.; Ortega, J.; Etxebarría, J. *Inorg. Chem.* **2009**, *48*, 6205–6210.
(20) Donnio, B.; Seddon, J. M.; Deschenaux, R. *Organometallics* **2000**, *19*, 3077–3081.
(21) Oriol, L.; Serrano, J. L. *Angew.Chem. Int. Ed.* **2005**, *44*, 6618–6621.
(22) Sessler, J. L.; Callaway, W. B.; Dudek, S. P.; Date, R. W.; Bruce, D. W. *Inorg. Chem.* **2004**, *43*, 6650–6653.
(23) Espinet, P.; Garcia-Orodea, E.; Miguel, J. A. *Chem. Mater.* **2004**, *16*, 551–555.
(24) Cardinaels, T.; Ramaekers, J.; Guillon, D.; Donnio, B.; Binnemans, K. *J. Am. Chem. Soc.* **2005**, *127*, 17602–17603.
(25) Binnemans, K.; Görller-Walrand, C. *Chem. Rev.* **2002**, *102*, 2303–2346.
(26) Donnio, B.; Guillon, D.; Bruce, D. W.; Deschenaux, R.; in *Comprehensive Coordination Chemistry II: From Biology to Nanotechnology*; McCleverty, J. A., Meyer, T. J., Ed.; Elsevier, Oxford, U.K., 2003; Vol. 7, Chapter 7.9, pp 357–627.
(27) Akagi, K.; Goto, H.; Bannai, H.; Piao, G.; Shirakawa, H. *Synth. Met.* **1997**, *86*, 1879–1880.
(28) Taubert, A. *Angew. Chem., Int. Ed.* **2004**, *43*, 5380–5382.
(29) Santoro, A.; Prokhorov, A. M.; Kozhevnikov, V. N.; Whitwood, A. C.; Donnio, B.; Williams, J. A. G.; Bruce, D. W. *J. Am. Chem. Soc.* **2011**, *133*, 5248–5251.
(30) Kim, J.-U.; Cha, S.-H.; Shin, K.; Jho, J. Y.; Lee, J.-C. *J. Am. Chem. Soc.* **2005**, *127*, 9962–9963.
(31) Lin, I. J. B.; Vasam, C. S. *J. Organomet. Chem.* **2005**, *690*, 3498–3512.
(32) Barberá, J.; Elduque, A.; Giménez, R.; Lahoz, F. J.; López, J. A.; Oro, L. A.; Serrano, J. L. *Inorg. Chem.* **1998**, *37*, 2960–2967.
(33) Holbrey, J. D.; Seddon, K. R. *Dalton Trans.* **1999**, 2133–2140.
(34) Trilla, M.; Pleixats, R.; Parella, T.; Blanc, C.; Dieudonné, P.; Guari, Y.; Man, M. W. C. *Langmuir* **2008**, *24*, 259–265.
(35) Lee, C. K.; Huang, H. W.; Lin, I. J. B. *Chem. Commun.* **2000**, 1911–1912.
(36) Lee, K. M.; Lee, Y.-T.; Lin, I. J. B. *J. Mater. Chem.* **2003**, *13*, 1079–1084.
(37) Yazaki, S.; Funahashi, M.; Kagimoto, J.; Ohno, H.; Kato, T. *J. Am. Chem. Soc.* **2010**, *132*, 7702–7708.
(38) Dobbs, W.; Heinrich, B.; Bourgogne, C.; Donnio, B.; Terazzi, E.; Bonnet, M.-E.; Stock, F.; Erbacher, P.; Bolcato-Bellemin, A.-L.; Douce, L. *J. Am. Chem. Soc.* **2009**, *131*, 13338–13346.
(39) Bowlas, C. J.; Bruce, D. W.; Seddon, K. R. *Chem. Commun.* **1996**, 1625–1626.
(40) Lee, C. K.; Peng, H. H.; Lin, I. J. B. *Chem. Mater.* **2004**, *16*, 530–536.
(41) Hardacre, C.; Holbrey, J. D.; McCormac, P. B.; McMath, S. E. J.; Nieuwenhuyzen, M.; Seddon, K. R. *J. Mater. Chem.* **2001**, *11*, 346–350.
(42) Lee, K. M.; Lee, C. K.; Lin, I. J. B. *Angew. Chem., Int. Ed.* **1997**, *36*, 1850–1852.
(43) Lee, C. K.; Chen, J. C. C.; Lee, K. M.; Liu, C. W.; Lin, I. J. B. *Chem. Mater.* **1999**, *11*, 1237–1242.
(44) Lee, C. K.; Vasam, C. S.; Huang, T. W.; Wang, H. M. J.; Yang, R. Y.; Lee, C. S.; Lin, I. J. B. *Organometallics* **2006**, *25*, 3768–3775.
(45) Camerel, F.; Ziessel, R.; Donnio, B.; Bourgogne, C.; Guillon, D.; Schmutz, M.; Iacovita, C.; Bucher, J.-P. *Angew. Chem., Int. Ed.* **2007**, *46*, 2659–2662.
(46) Tam, A. Y.-Y.; Wong, K. M.-C.; Wang, G.; Yam, V. W.-W. *Chem. Commun.* **2007**, 2028–2030.
(47) Estroff, L. A.; Hamilton, A. D. *Chem. Rev.* **2004**, *104*, 1201–1218.
(48) Xing, B.; Choi, M. F.; Xu, B. *Chem. Commun.* **2002**, *4*, 362–363.
(49) Terech, P.; Weiss, R. G. *Chem. Rev.* **1997**, *97*, 3133–3159.
(50) van Esch, J. H.; Feringa, B. L. *Angew. Chem., Int. Ed.* **2000**, *39*, 2263–2266.
(51) Das, A.; Ghosh, S. *Chem. Commun.* **2011**, *47*, 8922–8924.
(52) Ostuni, E.; Kamaras, P.; Weiss, R. G. *Angew. Chem., Int. Ed.* **1996**, *35*, 1324–1326.
(53) George, M.; Weiss, R. G. *Acc. Chem. Res.* **2006**, *39*, 489–497.
(54) McDonagh, C.; MacCraith, B. D.; McEvoy, A. K. *Anal. Chem.* **1998**, *70*, 45–50.
(55) Pérez, A.; Serrano, J. L.; Sierra, T.; Ballesteros, A.; Saá, D.; Barluenga, J. *J. Am. Chem. Soc.* **2011**, *133*, 8110–8113.
(56) Kato, T. *Science* **2002**, *295*, 2414–2418.
(57) Liu, Y.-R.; He, L.; Zhang, J.; Wang, X.; Su, C.-Y. *Chem. Mater.* **2009**, *21*, 557–563.
(58) Holtz, J. H.; Asher, S. A. *Nature* **1997**, *389*, 829–832.
(59) Yang, Z. M.; Ho, P. L.; Liang, G. L.; Chow, K. H.; Wang, Q. G.; Cao, Y.; Guo, Z. H.; Xu, B. *J. Am. Chem. Soc.* **2007**, *129*, 266–267.
(60) Vemula, P. K.; John, G. *Chem. Commun.* **2006**, 2218–2220.
(61) Gelman, F.; Blum, J.; Avnir, D. *J. Am. Chem. Soc.* **2000**, *122*, 11999–12000.
(62) Jeong, B.; Bae, Y. H.; Lee, D. S.; Kim, S. W. *Nature* **1997**, *388*, 860–862.
(63) Fages, F. *Angew. Chem., Int. Ed.* **2006**, *45*, 1680–1682.
(64) Piepenbrock, M.-O. M.; Lloyd, G. O.; Clarke, N.; Steed, J. W. *Chem. Rev.* **2010**, *110*, 1960–2004.
(65) Xing, B.; Choi, M. F.; Xu, B. *Chem.—Eur. J.* **2002**, *8*, 5028–5032.
(66) Tam, A. Y.-Y.; Wong, K. M.-C.; Yam, V. W.-W. *J. Am. Chem. Soc.* **2009**, *131*, 6253–6260.
(67) Lam, S.-T.; Wang, G.; Yam, V. W.-W. *Organometallics* **2008**, *27*, 4545–4548.
(68) Klawonn, T.; Gansäuer, A.; Winkler, I.; Lauterbach, T.; Franke, D.; Nolte, R. J. M.; Feiters, M. C.; Börner, H.; Hentschel, J.; Dötz, K. H. *Chem.Commun.* **2007**, 1894–1895.
(69) Bühler, G.; Feiters, M. C.; Nolte, R. J. M.; Dötz, K. H. *Angew. Chem., Int. Ed.* **2003**, *42*, 2494–2497.
(70) Tu, T.; Assenmacher, W.; Peterlik, H.; Weisbarth, R.; Nieger, M.; Dötz, K. H. *Angew. Chem., Int. Ed.* **2007**, *46*, 6368–6371.
(71) Hui, J. K.-H.; Yu, Z.; MacLachlan, M. J. *Angew. Chem., Int. Ed.* **2007**, *46*, 7980–7983.
(72) Zhang, J.; Xu, X.; James, S. L. *Chem. Commun.* **2006**, 4218–4220.
(73) Wei, Q.; James, S. L. *Chem. Commun.* **2005**, 1555–1556.
(74) Yamada, Y. M. A.; Maeda, Y.; Uozumi, Y. *Org. Lett.* **2006**, *8*, 4259–4262.
(75) Wang, H. M. J.; Lin, I. J. B. *Organometallics* **1998**, *17*, 972–975.
(76) Lin, J. C. Y.; Huang, R. T. W.; Lee, C. S.; Bhattacharyya, A.; Hwang, W. S.; Lin, I. J. B. *Chem. Rev.* **2009**, *109*, 3651–3598.
(77) Nielsen, D. J.; Cavell, K. J.; Skelton, B. W.; White, A. H. *Inorg. Chim. Acta* **2003**, *352*, 143–148.
(78) Lee, H. M.; Chiu, P. L.; Hu, C. H.; Lai, C. L.; Chou, Y. C. *J. Organomet. Chem.* **2005**, *690*, 403–414.
(79) Özdemir, İ.; Özcan, E. Ö.; Günal, S.; Gürbüz, N. *Molecules* **2010**, *15*, 2499–2508.
(80) Lee, K. M.; Chen, J. C. C.; Huang, C. J.; Lin, I. J. B. *CrystEngComm.* **2007**, *9*, 278–281.
(81) Chen, S. C.; Hsueh, H. H.; Chen, C. H.; Lee, C. S.; Liu, F. C.; Lin, I. J. B.; Lee, G. H.; Peng, S. M. *Inorg. Chim. Acta* **2009**, *362*, 3343–3350.
(82) Pregosin, P. S.; Anil Kumar, P. G.; Fernández, I. *Chem. Rev.* **2005**, *105*, 2977–2998.
(83) Cussler, E. L. *Diffusion: Mass Transfer in Fluid Systems*; Cambridge University Press: Cambridge, 1984.

(84) Saito, Y.; Hirai, K.; Murata, S.; Kishii, Y.; Kii, K.; Yoshio, M.; Kato, T. *J. Phys. Chem. B* **2005**, *109*, 11563−11571.
(85) Dobson, D. P.; Brodholt, J. P.; Vočadlo, L.; Crichton Mol., W. A. *Phys.* **2001**, *99*, 773−777.
(86) Kholodenko, A. L.; Douglas, J. F. *Phys. Rev. E* **1995**, *51*, 1081−1090.
(87) Dimitrova, Y.; Daskalova, L. I. *Spectrochim. Acta, Part A* **2009**, *71*, 1720−1727.
(88) Shen, Y.-T.; Li, C.-H.; Chang, K.-C.; Chin, S.-Y.; Lin, H.-A.; Liu, Y.-M.; Hung, C.-Y.; Hsu, H.-F.; Sun, S.-S. *Langmuir* **2009**, *25*, 8714−8722.
(89) Snyder, R. G.; Strauss, H. L.; Elliger, C. A. *J. Phys. Chem.* **1982**, *86*, 5145−5150.
(90) Binder, H.; Anikin, A.; Lantzsch, G.; Klose, G. *J. Phys. Chem. B* **1999**, *103*, 461−471.
(91) Park, H. K.; Ha, T. H.; Kim, K. *Langmuir* **2004**, *20*, 4851−4858.

dx.doi.org/10.1021/ic2011343 | *Inorg. Chem.* 2012, 51, 98−108